Topological Analysis of the Experimental Electron Density in Multiferroic Antiferromagnet $Ba_2MnGe_2O_7$

Rajesh Dutta[1,2], Henrik Thoma[1,2], Dmitry Chernyshov[3], Bálint Náfrádi[4], Takatsugu Masuda[5], Armin Kriele[6], and Vladimir Hutanu[1,2]

[1]Institut für Kristallographie, RWTH Aachen Universität, 52066 Aachen, Germany
[2]Jülich Centre for Neutron Science at Heinz Maier-Leibnitz Zentrum, 85747 Garching, Germany
[3]Swiss-Norwegian Beam Lines at ESRF, rue Jules Horowitz, FR-38042 Grenoble Cedex 9, France
[4]EPFL, Laboratory of Nanostructures and Novel Electronic Materials, 1015 Lausanne, Switzerland
[5]International Graduate School of Arts and Sciences, Yokohama City University, Yokohama, Kanagawa 236-0027, Japan
[6]German Engineering Materials Science Centre at MLZ, Helmholtz-Zentrum Geesthacht, 85748 Garching, Germany

In the field of magnetoelectric coupling, especially via the spin dependent metal-ligand *d-p* hybridization mechanism found in multiferroic $Ba_2MGe_2O_7$ (*M* = Mn, Co), a detailed knowledge of the microscopic structural parameters is essential, also for the theoretical modeling. In this article, we report a systematic structural study of $Ba_2MnGe_2O_7$ single crystal under varying temperature between 110 to 673 K using non-destructive *in-situ* single crystal synchrotron radiation diffraction. The maximum entropy method was applied to the X-ray diffraction data for the determination of the deformation in the electron density and the orbital hybridization between the *3d* of Mn and *2p* of O in the Mn−O bond. Within this entire temperature range, the structure was described in a single crystallographic space group $P\bar{4}2_1m$ and no structural phase transition has been detected. Interestingly, the forbidden reflections, which arise from multiple diffraction so called "Renninger effect", were observed at all temperatures without any symmetry lowering. The changes in the structural parameters (bond-lengths, bond-angles, anisotropic displacement parameters and electron density distributions of the atoms) with temperature are revealed, helping to understand some aspects comprising orbital hybridization in multiferroic $Ba_2MnGe_2O_7$.

***Index Terms*—Multiferroics, Antiferromagnet, X-ray diffraction, Renninger effect, *d-p* hybridization, electron density distribution**

I. Introduction

MULTIFERROIC melilite-type germanates such as $Ba_2MGe_2O_7$ (*M* = Mn, Co and Cu) are potential candidates for studying exotic quantum phenomena including low-energy magnetic, electronic and structural correlations along with the magnetoelectric effect [1–5]. There have been studies in search for tunable magnetic structures depending on the type of spin-orbit coupling (Rashba-Dresselhaus) with broken spatial inversion symmetry (SIS) [6, 7]. When SIS is broken, an antisymmetric spin exchange called Dzyaloshinskii–Moriya interaction (DMI) appears and has been observed in the noncentrosymmetric spin-5/2 antiferromagnet (AFM) $Ba_2MnGe_2O_7$ with space group $P\bar{4}2_1m$ below the Néel temperature ($T_N = 4$ K) [2, 5]. The more dominant component (in- or out-of-plane) of the DMI decides about the nature of the spin texture, but also the interplay with a magnetic field and the single-ion anisotropy plays a crucial role. Both, the weak uniform in-plane and the strong staggered out-of-plane component of the DMI exist in the square planner AFMs $Ba_2MnGe_2O_7$ and $Ba_2CoGe_2O_7$, whereas the former is strong in the case of the cycloidal AFM $Ba_2CuGe_2O_7$ [5, 8]. Recently, two-dimensional (2D) Dresselhaus antiferromagnet is actually realized in $Ba_2MnGe_2O_7$, where the microwave non-reciprocity is indeed observed [9] which means a possible existence of a strong in-plane DMI. This brings into discussion whether the both components of the DMI are correlated in $Ba_2MnGe_2O_7$.

It has been suggested that the spontaneous electric polarization in $Ba_2MnGe_2O_7$ arises due to the spin-dependent *d-p* hybridization mechanism between the transition metal *3d* and the ligand *2p* orbitals rather than spin current or magnetostriction mechanism similar to its sister compound $Ba_2CoGe_2O_7$ [5, 10]. While both compounds are exhibiting a similar non-centrosymmetric tetragonal nuclear structure with space group $P\bar{4}2_1m$ (n.113) below the corresponding T_N, they differ from each other mainly by their local spin microstructure and the type of Heisenberg exchange interactions [5, 11]. In $Ba_2MnGe_2O_7$, the interplane exchange coupling is antiferromagnetic ($J > 0$) doubling the magnetic unit cell along *c*-axis, whereas it is ferromagnetic ($J < 0$) in $Ba_2CoGe_2O_7$. In the last decades, the true symmetry of the nuclear and magnetic structures of multiferroic $Ba_2MnGe_2O_7$ and $Ba_2CoGe_2O_7$ has been studied via single crystal neutron and synchrotron X-ray diffraction at 10 K and RT [12–15]. These studies revealed, that observed weak symmetry extinct superstructure reflections are indeed originating from multiple diffraction, the so called "Renninger effect" [16] and there is no further symmetry lowering. But there is no single report on any structural phase transition if existent in these materials from high-T to below T_N.

It is crucial to investigate the detailed structural evolution with temperature to extract the structural parameters as function of the temperature for further justification whether the structure is correlated with the following microscopic physical phenomena: (1) the spin-dependent *d-p* hybridization mechanism, involving the coupling between the transition metal ions and the ligand oxygen atoms, strongly depending on the corresponding *Mn*-O bond-length and the bond direction inside the MnO_4 tetrahedron, see Fig. 1(d); (2) the induced electric polarization under external magnetic field which has been detected even at 50 K $> T_N$ in $Ba_2MnGe_2O_7$ [5]; and (3) most importantly, the induced local electric field in the MnO_4 tetrahedron and its distortion under temperature which may affect the low-energy crystal-electric field (CEF) excitations as

Corresponding author: R. Dutta (email: rajesh.dutta@frm2.tum.de).
Corresponding author: V. Hutanu (email: vladimir.hutanu@frm2.tum.de).

well as the pseudo-spin orbit coupling of magnons governing from uniform DMI. Therefore, in this sense, a significant step towards the understanding of the atomic arrangement and the physical properties of a material is the knowledge of how the electronic structure and the different chemical bonds present themselves at the microscopic scale. Experimentally, a portion of the electronic structure can therefore be identified from electron density maps obtained from X-ray diffraction experiments.

II. Experimental Methods and Data Treatment

High quality single crystals of $Ba_2MnGe_2O_7$ were grown by the floating-zone technique and characterized in previous studies [2, 12]. For the use in X-ray diffraction, tiny needle shaped samples were prepared with 50 μm in diameter and 200 μm long. *In-situ* synchrotron radiation (SR) single-crystal X-ray diffraction data were collected at the Swiss-Norwegian beamline (SNBL) BM01A [17] at the European radiation synchrotron facility (ESRF), Grenoble, France, on a Dectris Pilatus 2 M area detector, using a wavelength (λ) of 0.6974 Å. To collect a full three-dimensional volume of reciprocal space, the sample was rotated 360° with a step size of 0.1°. 2D diffraction images were recorded with an exposure of 0.1 s for each crystal rotation angle. The temperature was controlled and monitored with a gas heat blower for the high temperature measurement up to 673 K. A cold nitrogen blower from Oxford Cryostream was used for the low temperature data collection down to 110 K. The SNBL Toolbox was used for image preprocessing [17] and preparing the input parameter files. Then, an intial lattice refinement and 2D reciprocal space maps of the scattering intensity were reconstructed using the CrysAlisPRO software package [18]. The structure refinements were carried out using the Jana2006 software package [19]. The experimental three-dimensional electron density distribution (EDD) was reconstructed via the maximum entropy method (MEM) using Dysnomia [20] with a high-resolution grid (128×128×128 pixels) and the EDDs were visualized via VESTA [21]. The input files for the MEM analysis were prepared from JANA2006 after a Rietveld refinement. Finally, the graphics have been prepared using the *python matplot library* and OriginPRO.

III. Results and Discussion

A. *In-situ temperature dependent diffraction study*

Figure 1 (a,b) illustrate the full unit cell of $Ba_2MnGe_2O_7$ in the $P\bar{4}2_1m$ setting at RT. Two types of MnO_4 tetrahedron are observed in which the upper oxygen bonds make an angle $\mathcal{K}$ with the [110] diagonal. This parameter $\mathcal{K}$ plays an important role in determining the induced electric polarization (P) via the *d-p* hybridization mechanism. The MnO_4 tetrahedrons are interconnected with a corner shared GeO_4 tetrahedron. Atomic displacement parameters (ADP) for all atoms have been extracted after performing a Rietveld refinement on the data collected at RT. The results are shown in Fig. 1(c) and nicely resemble the neutron data in Sazonov et al. [12]. We will compare and discuss the ADP for different temperatures in the next section. The 2D reconstructed reciprocal maps of (0KL) planes obtained from SR-diffraction at various temperatures are shown in Fig. 2. All the reflections have been indexed using the $P\bar{4}2_1m$ space group except the reflections marked in white circles on the (0K0) or equivalent (H00) axis where

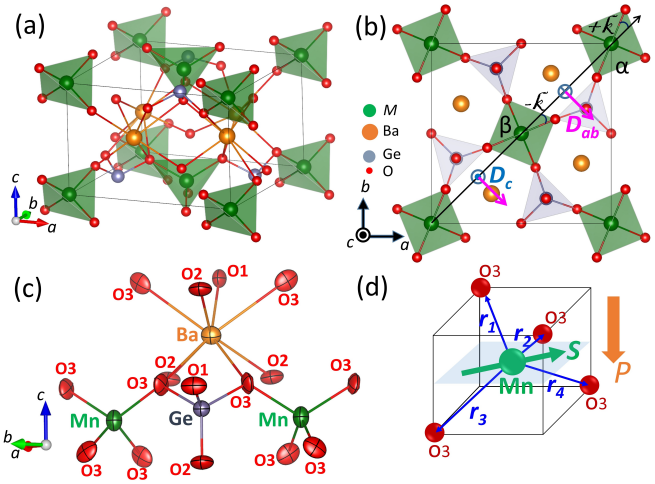

Fig. 1. Structure of $Ba_2MnGe_2O_7$ at RT. (a) Chemical unit cell. (b) Projected unit cell along the c-axis. Staggered out-of-plane components of DMI, $D_{c(+,-)}$ are represented as dotted and crossed blue circles respectively. Uniform components D_{ab} are shown as pink arrows. Two different arrangements of the MnO_4 tetrahedron α and β are shown. The angle ($\pm\mathcal{K}$) between the [110] diagonal and the bond made of upper two oxygen atoms in MnO_4 tetrahedron is marked. (c) Obtained ADP ellipsoids of all atoms from structure refinement are presented. (d) Schematic representation of Mn-O bond direction and Mn^{2+} spin inside the MnO_4 tetrahedron. Realized upward or downward induced electric polarization when the spin (S) is parallel to upper O3−O3 bond or lower O3−O3 bond, respectively.

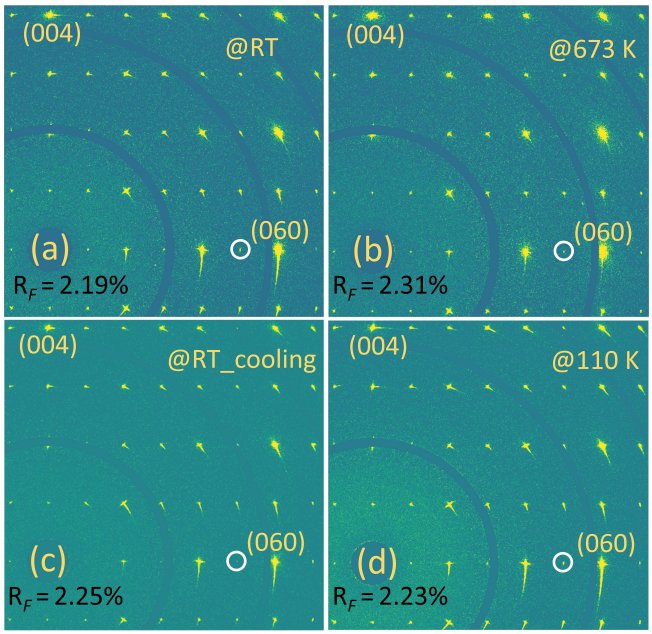

Fig. 2. 2D reconstructed (0KL) planes obtained at (a) RT, (b) 673 K, (c) RT after colling from 673 K and (d) 110 K. Dark bluish rings with zero pixel value are the detector gaps. White circles enclose the weak forbidden reflections. R_F indicates the Rietveld refinement R-factor based on the structure factor (F) for the corresponding temperature.

H,K = odd. These symmetry extinct reflections are nothing but forbidden peaks originated from Renninger effect, present at entire temperature range from 673 to 110 K and 10^4 times less in intensity compare to fundamental Bragg reflections. No extra reflections are observed compared to the RT phase indicating no symmetry lowering of the structure in an average scale. Therefore, we confirm that no structural phase transition takes place in $Ba_2MnGe_2O_7$ within the studied temperature range. Beside this, asymmetric diffuse tails are observed mainly around (0K0)-type reflections at lower d-values and it may come from sample mosaicity and sample surface effect,

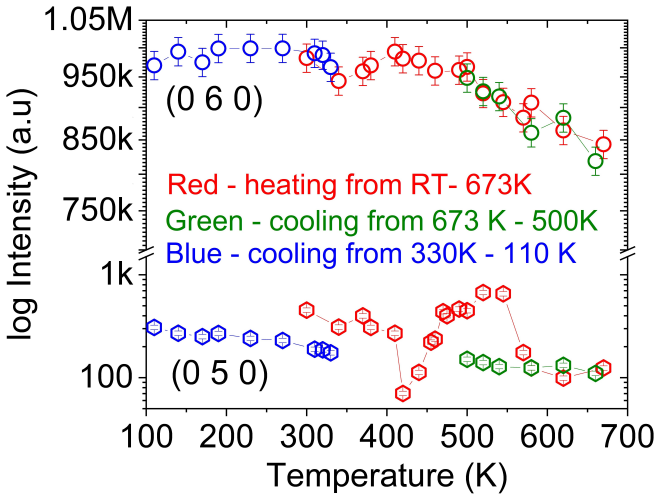

Fig. 3. Evolution of the integrated intensities of main Bragg reflection (060) and forbidden reflection (050) as function of temperature. Heating and cooling are indicated with different colors.

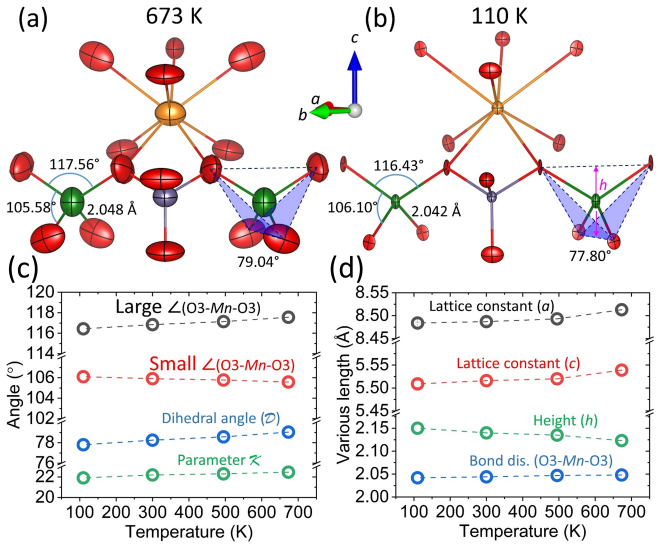

Fig. 4. (a-b) ADP ellipsoids of $Ba_2MnGe_2O_7$ obtained at 673 K and 110 K, respectively. Blue shades enclose the dihedral angle $\mathcal{D}$. Colors and labels of the atoms are the same as in Fig. 1(c). Evolution of various characteristic angles (c) and lengths (d) as function of the temperature.

but are not likely thermal diffuse scattering. The intensities of one of the strongest main structural reflection (060) and forbidden reflection (050) are plotted in Fig. 3 for different temperatures. The main reflection shows a reversible behavior during temperature rising (red circles) and cooling (green circles) and stays almost flat at the level of the RT phase during further cooling (blue circles). In contrast, the forbidden peak shows a scattered behavior typical for Renninger scattering.

In a local scale, the changes in the bond lengths, angles and anisotropic ADPs are identified with the change in temperature. Figure 4 shows the detailed comparison of the structural parameters obtained by Rietveld refinement. The dihedral angle ($\mathcal{D}$), enclosed by the two blue shaded triangular sides in Fig. 4(a,b), differs at these two temperature and therefore, corresponding height (h) which is indicated by a magenta arrow. The obtained characteristic parameter $\mathcal{K} \approx 22°$ in $Ba_2MnGe_2O_7$ is similar to the value (24°) found in $Ba_2CoGe_2O_7$ [13]. However, the change in $\mathcal{K}$ between 110 and 673 K is quite small $\sim 3\%$. The ADP ellipsoids of all atoms are enlarged at 673 K as expected from high temperature effects. Whereas at 110 K the scenario is different, especially the O3 atoms in the MnO_4 tetrahedron are shrank peculiarly along a certain direction. This already gives a hint towards possible changes in the electron density of O3 atoms with temperature.

B. Maximum entropy method and topological analysis

The MEM is a powerful way to obtain electron density information from diffraction data by maximizing the information entropy (S) under several constraints by iterative procedures. The MEM is also more accurate for the reconstruction of electron densities than using inverse Fourier transforms, because it overcomes information losses (experimental noise) and is capable of estimating structure factors of high-Q reflections that have not been measured experimentally, therefore, the termination effect is less serious in MEM analysis. Here, in Dysnomia the formalism of Collins [22] based on Jaynes's expression of S [23] and the Limited-memory Broyden-Fletcher-Goldfarb-Shannon (L-BFGS) algorithm [24] are used to reconstruct the electron density maps by using X-ray diffraction data.

Further more, using VESTA, topological analysis of the experimental $\rho(\mathbf{r})$ has been carried out via calculating the Laplacians of the electron densities $\nabla^2\rho(\mathbf{r})$, the electronic kinetic-energy densities G($\mathbf{r}$), the electronic potential-energy densities V($\mathbf{r}$), and the total electronic-energy densities H($\mathbf{r}$) according to Tsirelson's procedures [25]. Such topological parameters at $\mathbf{r}_{bcp}$ provide a quantitative description of bonding nature in organic and inorganic crystalline solids. $\mathbf{r}_{bcp}$ denotes the *bond-critical-point* (*bcp*) located on the bonds between pair of atoms where the gradient vector field $\nabla\rho(\mathbf{r}) = 0$. Bader & Beddall's virtual theorem [26] shows that local concentrations ($\nabla^2\rho(\mathbf{r}) < 0$) and depletions ($\nabla^2\rho(\mathbf{r}) > 0$) of the electron density are connected with the electronic-energy density as

$$2G(\mathbf{r}) + V(\mathbf{r}) = (\hbar^2/4m)\nabla^2\rho(\mathbf{r}) \quad (1)$$

and

$$H(\mathbf{r}) = G(\mathbf{r}) + V(\mathbf{r}) \quad (2)$$

As the responsible for the electric polarisation in $Ba_2MnGe_2O_7$ *d-p* hybridisation takes place in the MnO_4 tetrahydron, in this study we concentrate mainly on this part of the unit cell. Figure 5 displays the reconstructed via MEM experimental $\rho(\mathbf{r})$ of one MnO_4 tetrahedrons at 673, 300 and 110 K. At 300 K, $\rho(\mathbf{r})$ of Mn and O3 atoms are quite symmetric and spherical, whereas at low temperature those densities are distorted and the EDD surfaces are overlapped along the Mn−O3 bond showing the delocalized electron clouds. This can also be inferred from the graphical representation of the 1D $\rho(\mathbf{r})$ profile between the Mn−O3 bond shown in Fig. 5(d). At 110 K, the minimum of the electron density (MED) $\rho_{min}(\mathbf{r})$ $\approx$ 1.12 e/Å^3 at *bcp* is slightly higher than 1.01 e/Å^3 and 0.72 e/Å^3 at 300 and 673 K, respectively. This behavior is expected since by lowering temperature towards the temperature where spontaneous electric polarization via *d-p* hybridization appears, more and more electron density gets significantly overlapped. Green curve for 673 K in Fig. 5(d) is shifted slightly towards right because of tiny increase of bond length. However, it should be noted that although the experimental $\rho(\mathbf{r})$ is a dynamical function and includes thermal effect, topological theory is still valid for dynamical EDD [25]. But, the effect of thermal motion on the topological properties are noticeable, e.g. thermal motion at 673 K strongly diminishes the curvature of the electron density in the interatomic region, while at 110

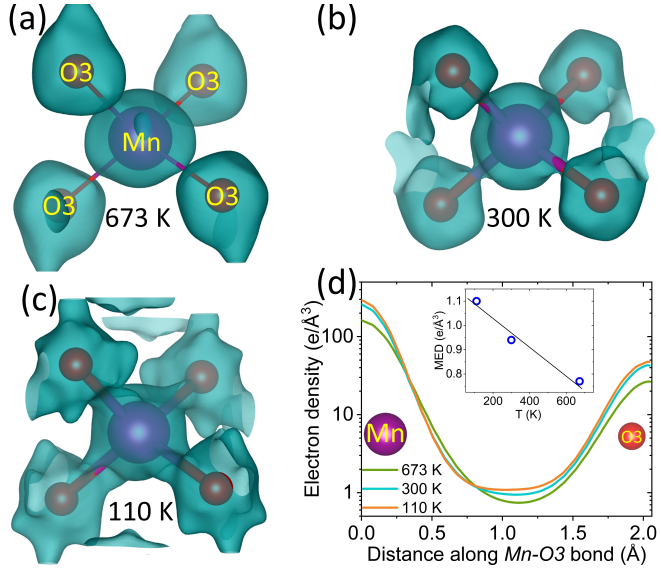

Fig. 5. (a-c) Three-dimensional electron density distribution of the MnO_4 tetrahedron in $Ba_2MnGe_2O_7$ obtained by MEM analysis at 673, 300 and 110 K, respectively. Isosurface density level is equal to 0.95 e/Å^3. (d) Variation of the one-dimensional electron density profile in logarithmic scale along the Mn−O3 bond in MnO_4 tetrahedron at 673, 300 and 110 K. Inset shows the minimum electron density (MED) at Mn−O3 bond as function of temperature.

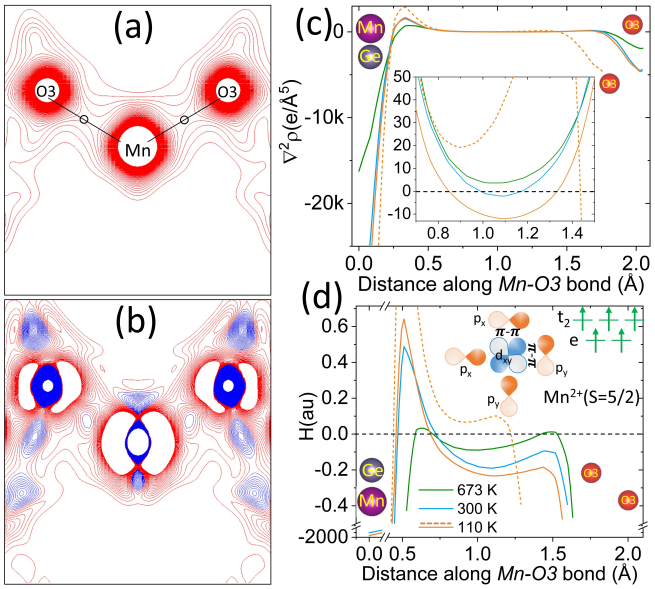

Fig. 6. 2D slice of experimental $\rho(\mathbf{r})$ (a) and $\nabla^2\rho(\mathbf{r})$ (b) obtained at 110 K in the MnO_4 tetrahedron, viewed along lower O3−O3 bond passing through origin. Black small circles indicate the *bcp* point. In (a,b) red and blue contour lines represent corresponding positive and negative values, respectively. In this linear mode, contour lines are drawn at every interval in data ranging from Min. to Max. The numerical value at the N^{th} line, F(N) is given by $F(N) = Min. + N \times Interval$. (c) Experimental 1D line profiles of $\nabla^2\rho(\mathbf{r})$ and (d) total electronic-energy densities H(**r**) along Mn−O3 bond. In (c,d) the orange dashed lines show similar profiles at 110 K for Ge−O3 bond. Inset in (c) shows the zoom section near *bcp*. In (d) a schematic of possible *3d-2p* orbital hybridization between t_2 and O2*p* has been presented for MnO_4 tetrahedra. Horizontal black dashed lines in (c,d) are eye guides to the zero level.

and 300 K, the curvature is quite flat where more overlapping takes place, see Fig. 5(d). The distance of the bond critical point to the nucleus can also be considered for an estimation of the ionic radius. The average Mn-*bcp* distance (0.98 Å) at 110 K is near to the 0.85 Å radius reported for the tetrahedrally coordinated Mn^{2+} [27] and is consistent with the charge slightly smaller than the ideal +2e.

In order to characterize the type of bond interactions, we have extracted the kinetic, potential and total electronic-energy density at *bcp* for different temperatures. The results are summarized in Fig. 6. From the topological treatment at *bcp*, it is well established that when $\nabla^2\rho(\mathbf{r}) < 0$, the electrons are shared by both nuclei, typical for shared or covalent atomic interactions, whereas $\nabla^2\rho(\mathbf{r}) > 0$ gives a closed-shell type interaction. However, the total electronic-energy density H(**r**) gives a more straightforward criterion for the recognition of the type of atomic interactions. In covalent or shared atomic interactions $H(\mathbf{r}) < 0$, independent of the sign of $\nabla^2\rho(\mathbf{r})$ whereas in closed-shell type interactions both $H(\mathbf{r}), \nabla^2\rho(\mathbf{r}) > 0$. Figure 6(a,b) shows the experimental $\rho(\mathbf{r})$ and $\nabla^2\rho(\mathbf{r})$ surrounding the Mn atoms obtained at 110 K. The EDD between the Mn−O3 bonds is symmetric and mirrored through the Mn atom, which means that the atomic interactions between the four Mn−O3 bonds in the MnO_4 tetrahedra are the same. In the Laplacian density map, the electrons are strongly concentrated at each nuclei position as usual but what is interesting to see is the value of $\nabla^2\rho(\mathbf{r})$ at *bcp*. This is why we have performed a 1D line cut along the Mn−O3 bond passing through the *bcp* and shown in Fig. 6(c). Due to large difference in the density level at nuclei and *bcp*, we present the zoom section near the *bcp* in the inset. At the same time we have extracted the total electronic-energy density H(**r**) which is presented in Fig. 6(d). Following the values and sign of H(**r**) and $\nabla^2\rho(\mathbf{r})$, it is noticeable that at 673 K, $H(\mathbf{r}) < 0$ but $\nabla^2\rho(\mathbf{r}) > 0$ indicating a partial covalent nature of the interaction between Mn-O3 bond while at 300 and 110 K both are negative i.e. pure covalent type interactions are established. However, $|\mathrm{H}(\mathbf{r})|_{110K} > |\mathrm{H}(\mathbf{r})|_{300K}$ and $\nabla^2\rho(\mathbf{r})_{110K} > \nabla^2\rho(\mathbf{r})_{300K}$ gives a hint that covalent nature is pronouncing below RT which is expected as the hybridization (overlapping) between *3d-2p* orbitals should occurs with lowering temperature. Tetrahedrally Mn^{2+} would prefer high spin (HS) ($e^2t_2^3$) state where both t_2 (d_{xy},d_{xz},d_{yz}) and e ($d_{x^2-y^2}$,d_{z^2}) orbitals are half-filled and contribute to the orbital mixing with O2*p* orbitals. Therefore, both side-to-side π-π and head-to-head σ-σ bonds are expected for the higher lying t_2 and lower lying e orbitals, respectively. For the π-π bonding situation a schematic is illustrated in Fig. 6(d).

Orbital overlap between Mn 3*d* and O 2*p* should reflects the interaction strength between the Mn and O3 atoms. But, one of the O3 atom is shared by both MnO_4 and GeO_4 tetrahedra, see Fig. 1(a). Are the O3 electron orbitals shared with Ge too especially since the length of Ge−O3 < Mn−O3? Fortunately, no, the atomic interactions between that Ge−O3 bond is purely closed-shell type (eventually ionic) since both $H(\mathbf{r}), \nabla^2\rho(\mathbf{r}) > 0$, as visible from the orange dashed curve in Fig. 6(c,d) obtained at 110 K. This is expected as the Ge^{4+} atoms have a closed-shell electronic configuration [Ar]$3d^{10}$ with no unpaired electrons. This indicates that the shared O3 atoms have only orbital overlapping with the Mn atoms. Nevertheless, electrostatic site potentials (ϕ) and the Madelung energy (E_M) per asymmetric unit have been deduced to have an indirect measure of the charge carrier distribution for all atom sites via the Fourier method adopted in MADEL as an external program in VESTA. The site potentials for Mn and O3 atoms are found to be -1.681 and 1.673 e/Å, respectively, indicating that the electrons from the O3 atoms are transferred towards the Mn atoms and E_M = -102.5 eV. Therefore, we can infer that suggested *d-p* hybridization mechanism in

course of the induced electric polarization (multiferroicity) is solely related with the MnO_4 tetrahedra. Also such *d-p*-π/σ hybridization is not related with drastic structural changes or phase transition, which have not been detected within the entire investigated temperature range, it might rather depend on the temperature mediated electron density deformation and of course is spin driven below T_N. In this scenario, it is also possible to conclude that the main contribution to the net electric polarization would be due to the Mn sites, whereas the Ge^{4+} [Ar]$3d^{10}$ and Ba^{2+} [Xe] sites have no contribution to the net electric polarization; this is because they only have core electrons and no valence electrons which would contribute to the electric polarization.

IV. Conclusion

An *in-situ* temperature dependent structural investigation in multiferroic $Ba_2MnGe_2O_7$ single crystal has been carried out using synchrotron X-ray diffraction in the temperature range from 110 to 673 K. Electron density maps, obtained experimentally by the maximum entropy method, were employed in the study of the microscopic electronic structure. The presented experimental electron density maps were obtained from the results of the structural Rietveld refinement of single crystal diffraction data mainly at 110, 300 and 673 K. MEM and *bond-critical-point* based topological analysis led to very precise findings about the crystal and electronic structures, as well as the type of the atomic interactions in $Ba_2MnGe_2O_7$ as function of temperature. The diffraction data revealed that, the structure of $Ba_2MnGe_2O_7$ remains a tetragonal lattice with $P\bar{4}2_1m$ symmetry without any structural phase transitions and sustaining of the forbidden Renninger reflections in the entire temperature range. The MEM study shows that bond strength and the significant orbital overlapping between Mn and O3 atoms increases with lowering the temperature from RT and the orbital hybridization, which is responsible for the total spontaneous electric polarizations below T_N, takes place mainly in the MnO_4 tetrahedron. Nonetheless, the deformation in the electron density in the MnO_4 tetrahedron along with the change in the topological structural parameters like, kinetic and potential energy density and especially the total electronic-energy density H(r), indicates to have a possible manifestation of the crystalline electric field (CEF) gradient as a function of the temperature. In other words, our study might benefit future investigations of the *T*-dependent microscopic electronic structure around the Néel temperature and therefore it would be interesting to investigate the CEF excitations in the frame of spin-orbit coupling and *d-p* hybridization.

Acknowledgment

We thank Vadim Diadkin for helping us with the measurement at beamline BM01, ESRF.

References

[1] J. Romhányi, F. Pollmann, and K. Penc, "Supersolid phase and magnetization plateaus observed in the anisotropic spin-$\frac{3}{2}$ heisenberg model on bipartite lattices," *Phys. Rev. B*, vol. 84, p. 2184427, Nov 2011.

[2] T. Masuda, S. Kitaoka, S. Takamizawa, N. Metoki, K. Kaneko, K. C. Rule, K. Kiefer, H. Manaka, and H. Nojiri, "Instability of magnons in two-dimensional antiferromagnets at high magnetic fields," *Phys. Rev. B*, vol. 81, p. 100402, Mar 2010.

[3] S. Miyahara and N. Furukawa, "Theory of magnetoelectric resonance in two-dimensional S = $\frac{3}{2}$ antiferromagnet $Ba_2CoGe_2O_7$ via spin-dependent metal-ligand hybridization mechanism," *Journal of the Physical Society of Japan*, vol. 80, no. 7, p. 073708, 2011.

[4] A. Zheludev, S. Maslov, G. Shirane, I. Tsukada, T. Masuda, K. Uchinokura, I. Zaliznyak, R. Erwin, and L. P. Regnault, "Magnetic anisotropy and low-energy spin waves in the dzyaloshinskii-moriya spiral magnet $Ba_2CuGe_2O_7$," *Phys. Rev. B*, vol. 59, pp. 11 432–11 444, May 1999.

[5] H. Murakawa, Y. Onose, S. Miyahara, N. Furukawa, and Y. Tokura, "Comprehensive study of the ferroelectricity induced by the spin-dependent *d-p* hybridization mechanism in $Ba_2XGe_2O_7$ (X = Mn, Co, and Cu)," *Phys. Rev. B*, vol. 85, p. 174106, May 2012.

[6] M. Kawano, Y. Onose, and C. Hotta, "Designing rashba–dresselhaus effect in magnetic insulators," *Communications Physics*, vol. 2, p. 27, March 2019.

[7] A. Manchon, H. C. Koo, J. Nitta, S. M. Frolov, and R. A. Duine, "New perspectives for rashba spin–orbit coupling," *Nature Materials*, vol. 14, p. 871, September 2015.

[8] T. Sato, T. Masuda, and K. Uchinokura, "Magnetic property of $Ba_2CoGe_2O_7$," *Physica B: Condensed Matter*, vol. 329-333, pp. 880 – 881, 2003, proceedings of the 23rd International Conference on Low Temperature Physics.

[9] Y. Iguchi, Y. Nii, M. Kawano, H. Murakawa, N. Hanasaki, and Y. Onose, "Microwave nonreciprocity of magnon excitations in the noncentrosymmetric antiferromagnet $Ba_2MnGe_2O_7$," *Phys. Rev. B*, vol. 98, p. 064416, Aug 2018.

[10] H. Murakawa, Y. Onose, S. Miyahara, N. Furukawa, and Y. Tokura, "Ferroelectricity induced by spin-dependent metal-ligand hybridization in $Ba_2CoGe_2O_7$," *Phys. Rev. Lett.*, vol. 105, p. 137202, Sep 2010.

[11] V. Hutanu, A. P. Sazonov, M. Meven, G. Roth, A. Gukasov, H. Murakawa, Y. Tokura, D. Szaller, S. Bordács, I. Kézsmárki, V. K. Guduru, L. C. J. M. Peters, U. Zeitler, J. Romhányi, and B. Náfrádi, "Evolution of two-dimensional antiferromagnetism with temperature and magnetic field in multiferroic $Ba_2CoGe_2O_7$," *Phys. Rev. B*, vol. 89, p. 064403, Feb 2014.

[12] A. Sazonov, V. Hutanu, M. Meven, G. Roth, R. Georgii, T. Masuda, and B. Náfrádi, "Crystal structure of magnetoelectric $Ba_2MnGe_2O_7$ at room and low temperatures by neutron diffraction," *Inorganic Chemistry*, vol. 57, no. 9, pp. 5089–5095, 2018.

[13] V. Hutanu, A. Sazonov, H. Murakawa, Y. Tokura, B. Náfrádi, and D. Chernyshov, "Symmetry and structure of multiferroic $Ba_2CoGe_2O_7$," *Phys. Rev. B*, vol. 84, p. 212101, Dec 2011.

[14] V. Hutanu, A. Sazonov, M. Meven, H. Murakawa, Y. Tokura, S. Bordács, I. Kézsmárki, and B. Náfrádi, "Determination of the magnetic order and the crystal symmetry in the multiferroic ground state of $Ba_2CoGe_2O_7$," *Phys. Rev. B*, vol. 86, p. 104401, Sep 2012.

[15] A. Sazonov, M. Meven, G. Roth, R. Georgii, I. Kézsmárki, V. Kocsis, Y. Tokunaga, Y. Taguchi, Y. Tokura, and V. Hutanu, "Origin of forbidden reflections in multiferroic $Ba_2CoGe_2O_7$ by neutron diffraction: symmetry lowering or renninger effect?" *Journal of Applied Crystallography*, vol. 49, no. 2, pp. 556–560, Apr 2016.

[16] M. Renninger, "Umweganregung, eine bisher unbeachtete wechselwirkungserscheinung bei raumgitterinterferenzen," *Zeitschrift für Physik*, vol. 106, no. 3, pp. 556–560, March 1937.

[17] V. Dyadkin, P. Pattison, V. Dmitriev, and D. Chernyshov, "A new multi-purpose diffractometer pilatus@snbl," *Journal of Synchrotron Radiation*, vol. 23, no. 3, pp. 825–829, May 2016.

[18] "CrysAlisPRO and Oxford Diffraction/Agilent Technologies UK Ltd., and Yarnton England."

[19] V. Petříček, M. Dušek, and L. Palatinus, "Crystallographic computing system JANA2006: General features," *Zeitschrift für Kristallographie - Crystalline Materials*, vol. 229, no. 5, pp. 345–352, 2014.

[20] K. Momma, T. Ikeda, A. A. Belik, and F. Izumi, "Dysnomia, a computer program for maximum-entropy method (mem) analysis and its performance in the mem-based pattern fitting," *Powder Diffraction*, vol. 28, no. 3, p. 184–193, 2013.

[21] K. Momma and F. Izumi, "*VESTA3* for three-dimensional visualization of crystal, volumetric and morphology data," *Journal of Applied Crystallography*, vol. 44, no. 6, pp. 1272–1276, Dec 2011.

[22] D. M. Collins, "Electron density images from imperfect data by iterative entropy maximization," *Nature*, vol. 298, pp. 49–51, July 1982.

[23] E. T. Jaynes, "Information theory and statistical mechanics," *Phys. Rev.*, vol. 106, pp. 620–630, May 1957.

[24] J. Nocedal, "Updating quasi-newton matrices with limited storage," *Math. Comp.*, vol. 35, pp. 773–782, July 1980.

[25] V. G. Tsirelson, "Topological analysis of the experimental electron density," *Canadian Journal of Chemistry*, vol. 74, no. 6, pp. 1171–1179, 1996.

[26] R. F. W. Bader and P. M. Beddall, "Virial field relationship for molecular charge distributions and the spatial partitioning of molecular properties," *The Journal of Chemical Physics*, vol. 56, no. 7, pp. 3320–3329, 1972.

[27] R. D. Shannon, "Revised effective ionic radii and systematic studies of interatomic distances in halides and chalcogenides," *Acta Crystallographica Section A*, vol. 32, no. 5, pp. 751–767, Sep 1976.